Hindawi
Mathematical Problems in Engineering
Volume 2023, Article ID 9632212, 15 pages
https://doi.org/10.1155/2023/9632212

Research Article

Waveform Prediction of Blade Tip-Timing Sensor Based on Kriging Model and Static Calibration Data

Liang Zhang, Qidi Wang, and Xin Li

Faculty of Mechanical Engineering and Automation, Liaoning University of Technology, Jinzhou, China

Correspondence should be addressed to Liang Zhang; zhangliang545238@163.com

Received 27 June 2022; Revised 9 January 2023; Accepted 28 January 2023; Published 17 February 2023

Academic Editor: Majid Niazkar

Blade tip clearance is an important parameter affecting the efficiency, stability, and safety of aero-engines. During the high-speed rotation of the blade, the blade tip clearance changes, which leads to changes in signal amplitude collected by the tip timing sensor. When the rotor is rotating at high speed, it is impractical to measure the tip-timing signal under each tip clearance. Aiming at the previous problems, a prediction method of blade tip-timing sensor waveform based on the combination of the Kriging model and static calibration data are proposed. The relationship between the output voltage of the tip timing sensor and the blade tip clearance and the angle of the blade tip cutting magnetic line is obtained by collecting the data of static calibration. Based on the collected static calibration experimental data and compared with the polynomial fit method and the RBF model, the accuracy of the Kriging model in predicting the waveform of the blade tip timing sensor was verified. The results show that the prediction accuracy of the Kriging model is basically the same as that of the RBF model, but the Kriging model has more advantages in predicting the waveform when the blade tip clearance is unknown. In contrast, the prediction accuracy of the polynomial fit is lower than that of the Kriging and RBF models, and the polynomial fit is prone to significant prediction errors.

1. Introduction

Rotor blades are the core component of an aero-engine, which are subjected to a variety of complex forces that generate vibrations during high-speed rotation [1]. Therefore, real-time monitoring of the vibration state of the blades is an effective method to ensure the safe operation of an aero-engine. During engine operation, factors such as thermal deformation, centrifugal deformation, and unbalanced rotor response would cause changes in tip clearance [2, 3]. Blade tip clearance refers to the radial distance between the tip of the rotor blade and the engine casing, which is an important parameter affecting the efficiency, stability, and safety of gas turbines [4]. Among them, the efficiency of the gas turbine is inversely proportional to the tip clearance. The larger the tip clearance, the larger the tip-leakage with an associated loss of high-energy gas and the lower the engine's efficiency [5]. Conversely, a smaller tip clearance may bring the risk of friction between the blade and the engine casing. Therefore, it is essential to monitor the blade tip clearance in real-time, give early warning to the failure of the blade, and ensure the smooth operation of the engine.

In recent years, more and more researchers have begun to dedicate themselves to the research on the blade tip clearance measurement of the engine. They have proposed several tip clearance measurement methods, including the probe method [6], optical fiber method [7], capacitance method [8], eddy current method [9], and microwave method [10]. Among them, the technical principles of different measurement methods are different, and each has its advantages and disadvantages. It is necessary to select an appropriate monitoring method according to different application environments.

Qi and Chen [11] used the finite element method to perform a numerical analysis of the blade tip clearance and obtained the variation law of the blade tip clearance during the working process of a specific type of aero-engine. However, it is not easy to accurately estimate the actual tip clearance in experimental measurements by obtaining the tip clearance results under different working conditions

through theoretical simulation under simplified conditions. Shang [12] proposed a tip clearance calibration technology combining radial and circumferential calibration. During the static circumferential calibration, the voltage at different relative spatial positions of the blade end face to the sensor probe end face was calibrated according to the time course. Shao [13] optimized the static calibration method and proposed a trigger pulse method. Combined with the static calibration data, the tip clearance value of the blade under dynamic undersampling conditions was obtained. The static calibration of the blade is usually carried out under some specific clearances. It takes a lot of time and effort to obtain a large amount of experimental data, and slight differences would cause large errors in the experimental results. Also, in dynamic experiments, it is very difficult to measure the pulse signal of each clearance as a reference. Jamia et al. [14] developed a quasi-static 3D finite element model of an electromagnetic field to simulate blade tip-timing applications to estimate the output from active and passive eddy current sensors. The effect of blade tip clearance and rotational speed on the accuracy of blade tip-timing measurement was shown through a parametric study. Cao et al. [15] proposed the short-time Fourier transform with adaptive window length, which extracted natural frequencies from a single blade tip-timing measurement based on a sampling-aliasing frequency map and corresponding engine order. Mandache et al. [16] developed a pulsed eddy current technique to detect engine blade and disk damage by monitoring blade tip displacement. Liu and Jiang [17] established a method that can correct the expected arrival time in the presence of torsional vibration based on the traditional blade tip-timing method, which improves the accuracy of blade vibration monitoring. Wu et al. [18] proposed a speed adjustment model-based blade tip clearance measurement method and constructed a geometric constraint equation to evaluate the accuracy of the blade tip clearance measurement.

Ariyarit et al. [19] investigated a multifidelity optimization technique for an efficient global optimization process using a hybrid agent model, which uses a Kriging method to construct local deviations and a radial basis function to construct a global model. It is used for the optimization of the aerodynamic design of helicopter blades to obtain maximum blade efficiency. Han and Görtz [20] proposed a hierarchical Kriging model, which can be applied to efficient aerodynamic analysis and shape optimization of aircraft. Bu et al. [21] used a hierarchical Kriging model for rotor optimization design, which improved the efficiency of the traditional Kriging model. Huang et al. [22] built an effective multifidelity surrogate model based on two independent high-fidelity and low-fidelity samples using a Co-Kriging method. Bailly and Bailly [23] applied the multifidelity optimization technique to the design of a helicopter rotor blade and verified that aerodynamic optimizations using a Co-Kriging surrogate model has advantages over the single-fidelity Kriging model.

Therefore, this paper proposes a method for predicting the waveform of the tip timing sensor based on the Kriging model and static calibration data. The relationship data between the output voltage of several groups of tip timing sensors and the tip clearance, and the angle of the blade cutting magnetic field line are measured in a static state. The waveform signals of different blade tip clearances are predicted, and the better prediction accuracy is obtained. The organization of this paper is as follows: Section 2 establishes a static calibration test bench and calibrates the relationship between the output voltage of the sensor and the blade tip clearance, the angle of the blade cutting the magnetic induction line based on the static calibration experiment, and the polynomial equation is fitted based on these relationships. The Kriging and the RBF models are established in Section 3. Section 4 verifies the prediction accuracy of the Kriging models, RBF model, and polynomial fitting method. Finally, the main conclusions of this article are given in Section 5.

2. Experimental Study on the Static Calibration of Blade Tip Clearance Measurement

2.1. Measurement Principle of the Eddy Current Method. The eddy current method uses metal cutting magnetic lines of force to generate magnetic field changes. The clearance measurement device comprises a probe and a detection circuit. The sensor probe is placed at a certain distance from the tip of the blade. When an alternating current is applied to the coil inside the probe, an alternating magnetic field is generated in the coil of the probe. When the blade under test is close to this magnetic field, an induced current is generated on the blade surface. At the same time, the eddy current field also generates an alternating magnetic field whose direction is opposite to the direction of the probe coil, resulting in a change in the equivalent impedance Z of the probe coil [24]. At this point, the functional expression of the equivalent impedance Z can be expressed as follows:

$$Z = f(\sigma, \mu, \omega, r, x), \tag{1}$$

where σ is the blade electrical conductivity, μ is the blade magnetic permeability, ω is the passing frequency, r is the size factor, and x is the tip clearance.

2.2. Building Eddy Current Sensor Static Calibration Test Bench. The static calibration test bench consists of the radial moving device and the circumferential rotating device, as shown in Figure 1. The eddy current sensor is mounted on the radial moving device. The XYZ three-axis displacement platform adjusts the position of the eddy current sensor so that the center of the eddy current sensor probe is aligned with the center of the blade tip and adjusts the tip clearance between the sensor probe and the blade. The blade is fixed on the disk and the disk is mounted on the R-axis rotation platform. The R-axis rotation platform adjusts the angle between the tip of the blade and the center of the eddy current sensor probe.

In this experiment, the parameters of the eddy current sensor and the blade are constant, so the size factor r of the coil, the electrical conductivity σ of the blade, the magnetic

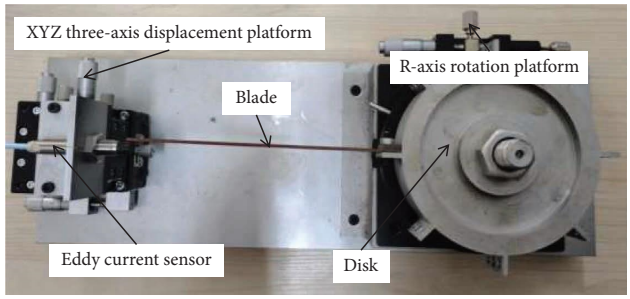

Figure 1: Static calibration test bench.

permeability μ of the blade, and the passing frequency ω are constant. Therefore, the coil impedance value Z of the eddy current sensor should only be related to the tip clearance x. The change in the coil impedance value Z of the eddy current sensor is changed to the change in the output voltage U by the conversion circuit. For the object whose measured surface is flat, with the center of the eddy current sensor probe surface, the diameter of the measured surface should be more than 1.5 times the diameter of the probe. In this measurement experiment, the thickness of the blade is only 2 mm, while the diameter of the eddy current sensor probe is 8 mm, the diameter of the eddy current sensor probe is much larger than the thickness of the blade. As a result, the output voltage U of the sensor is also different when the blade tip and the center of the eddy current sensor probe are in different relative circumferential positions. Therefore, the output voltage U of the eddy current sensor is affected by the tip clearance x, the blade thickness h, and the angle α of the blade cutting the magnetic induction lines [25]. Therefore, the output voltage U of the eddy current sensor is expressed as follows:

$$U = f(x, h, \alpha). \tag{2}$$

For a known blade, the blade thickness h is constant. Therefore, the output voltage U of the eddy current sensor can be expressed as follows:

$$U = f(x, \alpha). \tag{3}$$

According to equation (3), when the blade thickness h is known, the output voltage U of the eddy current sensor is only affected by the tip clearance x and the angle α of the blade cutting magnetic induction lines.

2.3. Experimental Scheme. Through the actual measurement of the static radial calibration experiment, the radial measurement range of the TR81 type eddy current displacement sensor is 0.1~0.55 mm under the condition that the blade is stationary [26]. The specific process for static circumferential calibration within this measurement range is as follows: first, we align the center of the eddy current sensor probe with the center of the blade tip to be measured, adjust the blade tip clearance, and keep it constant. Then, we use the R-axis rotation platform to rotate the blade to the edge of the eddy current sensor probe and record the scale of this position. Next, we rotate a fixed angle each time and record the output voltage value at each stop until it exceeds the measurement range of the eddy current sensor. Finally, we repeat the experiment in the range of 0.1~0.55 mm and complete the static circumferential calibration of the blade. The process of static circumferential calibration under different tip clearances is shown in Figure 2.

2.4. Static Calibration Experimental Study. First, we aligned the tip of the blade to the center of the eddy-current sensor probe and adjusted the tip clearance to 0.1 mm. Next, we adjusted the R-axis rotation platform so that the tip of the blade was gradually away from the center of the sensor probe, stopped when the measured voltage value was close to the lower limit of the sensor's measurement range, and recorded the angle as 0°. With 2.3′ as a step, the R-axis rotary platform rotated five scales and recorded the voltage value once. The rotation stopped when the vane rotated again to the lower limit of the sensor's measuring range. After measuring the experimental data under the tip clearance of 0.1 mm, the static circumferential calibration under each tip clearance was completed in sequence with a step size of 0.05 mm. The experiment was repeated five times for each blade tip clearance. The average of five experimental data was taken as the static circumferential calibration data under this blade tip clearance. The recorded data reflect the relationship between the output voltage U of the eddy current sensor and the blade tip clearance x, the angle α of the blade cutting the magnetic induction line. After getting all the data, data fitting was performed with the help of MATLAB to obtain the relationship curves of the output voltage U of the eddy current sensor and the blade tip clearance x, the angle α of the blade cutting the magnetic induction line. The static circumferential calibration curve of each blade tip clearance is shown in Figure 3.

As can be seen from Figure 3, the number of output voltage values collected by the eddy current sensor probe gradually decreases with the increase of the blade tip clearance x when the static circumferential calibration experiment is performed. This is because the range of magnetic field that the blade can cut to gradually decreases when the blade tip clearance x increases.

A polynomial fit to the data in Figure 3 is performed to obtain the functional relationship of the output voltage U of the eddy current sensor and the blade tip clearance x, the angle α of the blade cutting the magnetic induction line. The fitted curve is plotted as shown in Figure 4.

The polynomial equation obtained from the fitted curve is as follows:

$$U = f(x, \alpha) = -2647x^2 - 2.724\alpha^2 - 7060x + 192.8\alpha + 4.369x\alpha - 3779. \tag{4}$$

The square of the correlation coefficient of the fitted equation is 0.9981. However, equation (4) does not guarantee that all the collected sample points are on a curved surface, which is prone to significant prediction errors. Therefore, this article uses the Kriging model to predict the

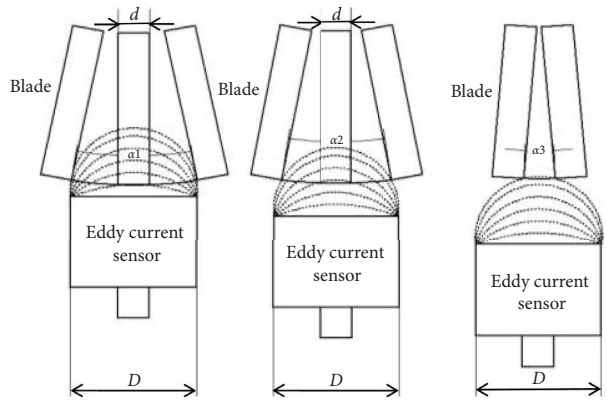

Figure 2: Static circumferential calibration of the blade.

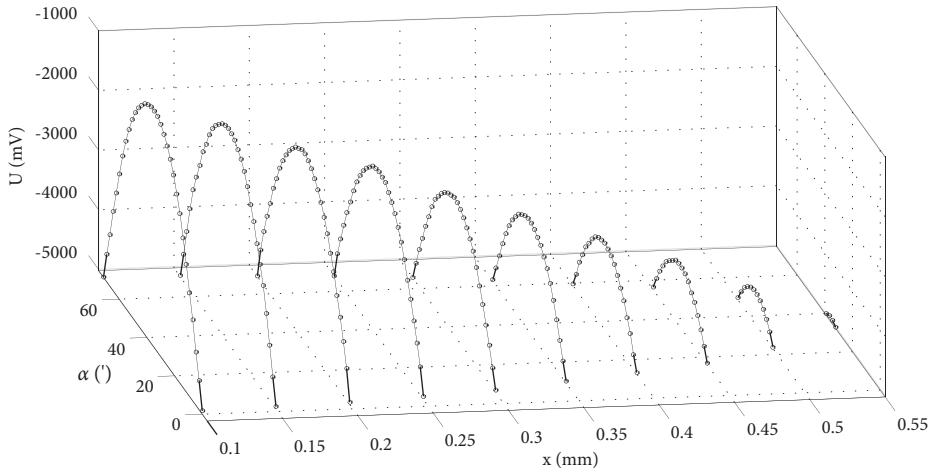

Figure 3: Static circumferential calibration curve of each blade tip clearance.

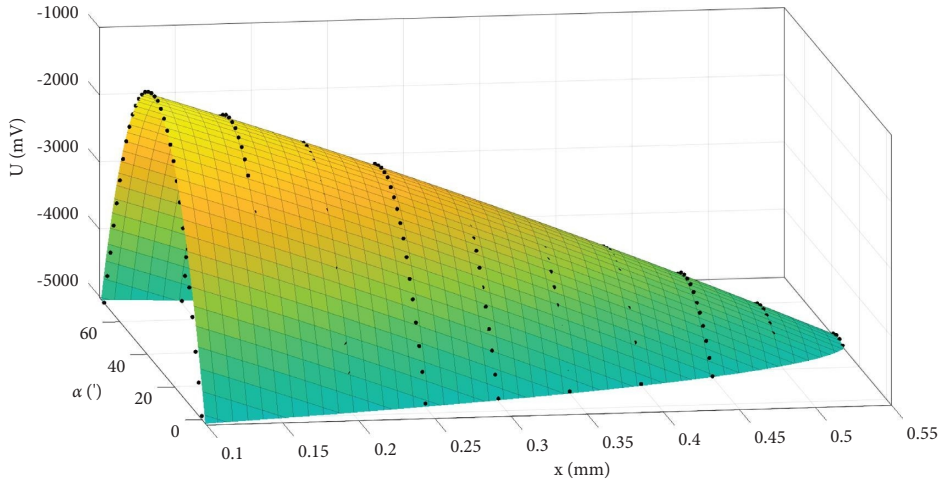

Figure 4: Fitted curve based on a polynomial function.

output voltage U of the eddy current sensor in relation to the blade tip clearance x and the angle α of the blade cutting the magnetic induction line.

3. Static Circumferential Calibration Curve Prediction Based on the Kriging Model

3.1. Kriging Model. The Kriging model, initially proposed in geostatistics, is a stochastic process-based proxy model that is now applied in reliability assessment [27, 28]. It is an optimal estimation method for finite localized variables based on theoretical analysis of variation function.

The Kriging model is a semiparametric interpolation technique that includes linear regression and nonparametric techniques. It generally consists of polynomial distribution and random distribution and can be written as follows:

$$y(x) = f(x) + z(x), \tag{5}$$

where $y(x)$ is fitted response function, $\beta = \begin{bmatrix} \beta_1 & \beta_2 & \cdots & \beta_p \end{bmatrix}^T$ is the regression coefficient, $f(x)$ is a known polynomial function that reduces $f(x)$ to a constant β in many cases, and $z(x)$ is a random distribution with nonzero covariance that obeys a normal distribution $N(0, \sigma^2)$; the covariance can be written as follows:

$$Cov\left[z(x_i), z\left(x_j\right)\right] = \sigma^2 R\left(x_i, x_j\right), \tag{6}$$

where σ^2 is the variance of $z(x)$ and $R(x_i, x_j)$ is the correlation function between x_i and x_j. In this article, the Gaussian function with better computational efficiency is chosen as the correlation function, which has the following form:

$$R\left(x_i, x_j\right) = \exp\left(-\sum_{k=1}^{m} \theta_k \left|x_i^k - x_j^k\right|^2\right), \tag{7}$$

where m is the number of design variables, θ_k is the correlation coefficient of the fitted model, and x_i^k and x_j^k are the kth component of the sample points x_i and x_j, respectively. The sample point correlation function matrix is as follows:

$$R = \begin{bmatrix} R(x_1, x_1) & \cdots & R(x_1, x_n) \\ \vdots & \ddots & \vdots \\ R(x_n, x_1) & \cdots & R(x_n, x_n) \end{bmatrix}, \tag{8}$$

where n is the number of sample points.

After determining the correlation function, $\widehat{y}(x)$ is the approximate response of $y(x)$. The expression containing the observation point x can be written in the following form:

$$\widehat{y}(x) = \widehat{\beta} + r^T(x) R^{-1}(y - f\widehat{\beta}), \tag{9}$$

where y is the column vector of sample points, including the observed response values for each design point, f is the column vector of sample points, f is the unit column vector when $f(x)$ is a constant, and $r^T(x)$ is the column vector of sample points, indicating the correlation between the observed points x and the sample points $(x_1, x_2, \ldots, x_n)$, expressed in the following form:

$$r^T(x) = \left[R(x, x_1), R(x, x_2), \cdots, R(x, x_n)\right]^T. \tag{10}$$

$\widehat{\beta}$ is the following assessment:

$$\widehat{\beta} = \left(f^T R^{-1} f\right)^{-1} f^T R^{-1} y. \tag{11}$$

When $f(x)$ is assumed to be a constant, $\widehat{\beta}$ is reduced to a scalar.

σ^2 is the variance estimate, which can be expressed as follows:

$$\widehat{\sigma}^2 = \frac{(y - f\widehat{\beta})^T R^{-1} (y - f\widehat{\beta})}{n}. \tag{12}$$

When $f(x)$ is assumed to be a constant, f is reduced to a unit column vector.

In equation (7), the maximum likelihood estimate of θ_k can be obtained from the maximum of equation (13). σ^2 and $|R|$ are both dependent variables of θ_k ($\theta_k > 0$):

$$-\frac{n \ln\left(\widehat{\sigma}^2\right) + \ln|R|}{2}. \tag{13}$$

By solving the k-dimensional nonlinear unconstrained optimization of equation (13), the best-fit Kriging model is acquired.

3.2. Building the Kriging Prediction Model. The Kriging interpolation algorithm is applied to predict the collected static calibration experimental data. Four Kriging prediction models with different numbers of collected sample points were constructed, as shown in Figures 5(a)–5(d). In Figures 5(a)–5(d), the sample point groups are 10, 6, 5, and 3, respectively. Figure 5(a) inputs all the data obtained from the static calibration experiment, and the predicting results of this model should theoretically be closest to the experimentally measured true values. Figure 5(b) experimental data for inputting blade tip clearance of 0.1 mm, 0.2 mm, 0.3 mm, 0.4 mm, 0.5 mm, and 0.55 mm, comparing the effect of sample point reduction on the prediction accuracy of the Kriging model. Figure 5(c) removes the experimental data of 0.55 mm from Figure 5(b) to observe the prediction accuracy of the Kriging model for waveforms outside the range of the collected blade tip clearance. Figure 5(d) retains only the experimental data of 0.1 mm, 0.3 mm, and 0.55 mm to observe whether the Kriging model still has high prediction accuracy when the number of collected sample points is few.

Meanwhile, in order to reflect the advantage of the Kriging model in predicting the waveform of the blade tip timing sensor, the RBF model is established at six sets of sample points, as shown in Figure 6. Moreover, the RBF model is compared with the Kriging model for prediction accuracy.

4. Validation of Kriging Model Prediction Accuracy

From equation (3), it can be seen that the output voltage U of the eddy current sensor is only related to the blade tip clearance x and the angle α of the blade cutting magnetic

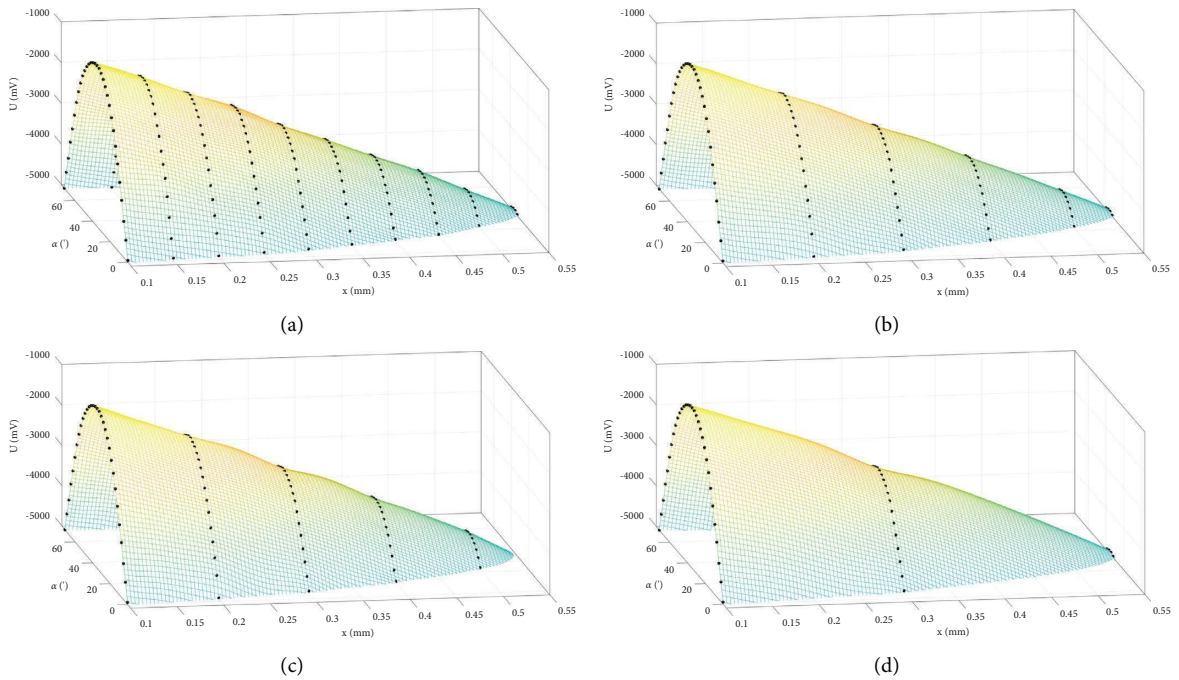

Figure 5: Kriging models with different number of sample point groups: (a) 10 sets of sample points, (b) 6 sets of sample points, (c) 5 sets of sample points, and (d) 3 sets of sample points.

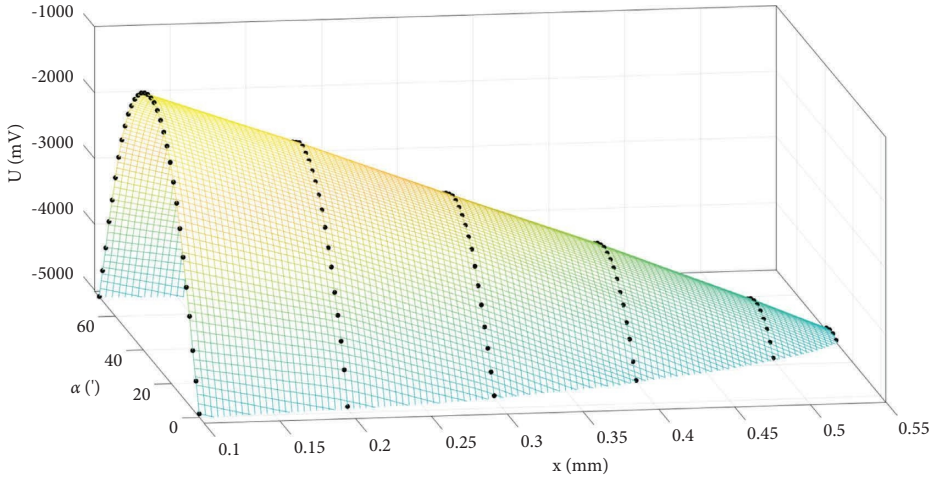

Figure 6: RBF model with 6 sets of sample points.

inductance line when other conditions have been determined. Suppose the angle α of the blade cutting magnetic induction line is kept unchanged, and only the distance between the blade and the blade tip timing sensor is changed. In that case, the static radial characteristic curve of the output voltage U of the eddy current sensor and the blade tip clearance x can be obtained. Conversely, by keeping the blade tip clearance x constant and changing only the angle α of the blade cutting the magnetic induction line, the static waveform under this blade tip clearance can be obtained.

4.1. Prediction of the Static Radial Characteristic Curve at the Specific Angle. Representative angles will be selected for prediction. The Kriging models, the RBF model, and the polynomial equation (4) are used for prediction when the angle α of the blade cutting magnetic field line is $17.825'$ and $35.65'$, respectively. When the angle α of the blade cutting the magnetic field line is $17.825'$, it means that the blade is in the middle position from the vertical center line of the eddy current sensor to the edge, and it is approximately half of the measured signal amplitude height. At this angle, if the blade tip clearance exceeds 0.45 mm, the blade cannot cut the magnetic field line of the eddy current sensor and cannot continue to obtain voltage. Therefore, the measurement range of the clearance at this angle is 0.1~0.45 mm. The comparison of the Kriging models prediction curves, the RBF model prediction curve, and the polynomial fit

prediction curve with the static radial characteristic curve obtained from the experimental data are shown in Figures 7(a)–7(c), and 7(f). As can be seen from Figures 7(a)–7(d), the prediction curves of the Kriging models with four different number of sample groups are basically the same, and they all have a high degree of coincidence with the static radial characteristic curves drawn from the experimental data. As shown in Figure 7(e), the polynomial fit prediction curve overlaps slightly less than the Kriging model with the static radial characteristic curve obtained from the experimental data. As shown in Figure 7(f), the RBF model has a high degree of agreement with the static radial characteristic curve derived from the experimental data.

The prediction errors are shown in Figure 8. As can be seen in Figure 8, when the angle α of the blade cutting the magnetic induction line is $17.825'$, the absolute errors predicted by the four Kriging models and the RBF model are less than 40 mV. The prediction accuracy of the RBF model is slightly lower than that of the Kriging model at the same number of sample point groups. However, the prediction errors are all within the measurement error range of the eddy current sensor, indicating that both Kriging and RBF models have good prediction accuracy at this angle. The absolute error of the polynomial fit prediction is less than 60 mV, which is also within the measurement error.

When the angle α of the blade cutting the magnetic field line is $35.65'$, the vertical center line of the blade coincides with the vertical center line of the eddy current sensor, and the peak value of the output voltage U of the eddy current sensor will be obtained at this position. The comparison of the Kriging models prediction curves, the RBF model prediction curve, and the polynomial fit prediction curve with the static radial characteristic curve obtained from the experimental data are shown in Figures 9(a)–9(f). The predicted curves of the Kriging model in Figures 9(a) and 9(b) are basically the same as the static radial characteristic curves obtained from the experimental data. Combined with Figures 7(a) and 7(b), it can be shown that even if a certain number of sample points are reduced, the prediction curves of the Kriging model do not change much. In Figure 9(c), when the tip clearance is 0.5~0.55 mm, the predicted point has an obvious turn. However, due to the correction of other prediction points, the prediction curve of the Kriging model does not change significantly. Suppose the prediction range of the tip clearance continues to increase, a relatively obvious error will occur, indicating that the accuracy of the Kriging model will be reduced when predicting points outside the sampling point range. The predicted curve of the Kriging model in Figure 9(d) is shifted somewhat relative to the static radial characteristic curve drawn from the experimental data. As can be seen in Figures 9(e) and 9(f), the polynomial fit prediction curve, the RBF model prediction curve, and the static radial characteristic curve obtained from the experimental data are in good agreement.

The prediction errors are shown in Figure 10. As can be seen from Figure 10, the absolute errors of the predictions of the Kriging model in Figures 9(a)–9(c) and the RBF model in Figure 9(f) are both minor, indicating that the Kriging model and the RBF model have good prediction accuracy. Moreover, under the same number of sample point sets, the prediction errors of the RBF model and the Kriging model under the same blade tip clearance are different. Still, the overall prediction accuracy is basically the same. However, the prediction errors of the Kriging model in Figure 9(d) increase significantly, indicating that the prediction accuracy of the Kriging model decreases when the number of groups of sample points is few. When the Kriging model had only three sets of sample points, the prediction accuracy of the polynomial fit was better than that of the Kriging model. Although the prediction accuracy of the polynomial fit is slightly lower than that of the Kriging models with other sample point numbers, the prediction error is also smaller, indicating that the polynomial fit has good accuracy in the prediction of static radial characteristic curves.

4.2. Prediction of the Static Circumferential Characteristic Curve at the Specific Tip Clearance. The static circumferential characteristic curves under two tip clearances of 0.15 mm and 0.2 mm were predicted based on the Kriging model, the RBF model, and the polynomial fit. The prediction accuracy of the Kriging models, the RBF model, and the polynomial fitting method is verified by comparison with static circumferential calibration curves. When the tip clearance x is 0.2 mm, the comparison of the Kriging models prediction curves, the RBF model prediction curve, and the polynomial fit prediction curve with the static circumferential calibration curve obtained from the experimental data are shown in Figures 11(a)–11(f). In Figures 11(a)–11(c), the static calibration data when the tip clearance is 0.2 mm have been input into the Kriging model. Therefore, the prediction curves of the Kriging models in Figures 11(a)–11(c) are highly consistent with the static circumferential calibration curve. There is a certain deviation between the static circumferential characteristic curve predicted by the Kriging model in Figure 11(d) and the static circumferential calibration curve. In this model, the static calibration data when the tip clearance is 0.2 mm is not input, but the number of sample point groups in this model is too few, which does not mean that the Kriging model is not accurate enough to predict the data that is not input. As shown in Figure 11(e), the polynomial fit prediction curves are in high agreement with the static circumferential calibration curve derived from the experimental data. In Figure 11(f), the static calibration data at the tip clearance of 0.2 mm have also been input into the RBF model. Therefore, the prediction curve of the RBF model is also highly consistent with the static circumferential calibration curve.

The prediction error comparison is shown in Figure 12. It can be seen from Figure 12 that when the tip clearance x is 0.2 mm, the prediction accuracy of the Kriging model in Figures 11(a)–11(c) is basically the same, and the absolute errors are all less than 20 mV. The prediction accuracy of the RBF model is slightly higher than that of the Kriging model at the same number of sample point groups, but the difference is slight. Moreover, the prediction errors are all

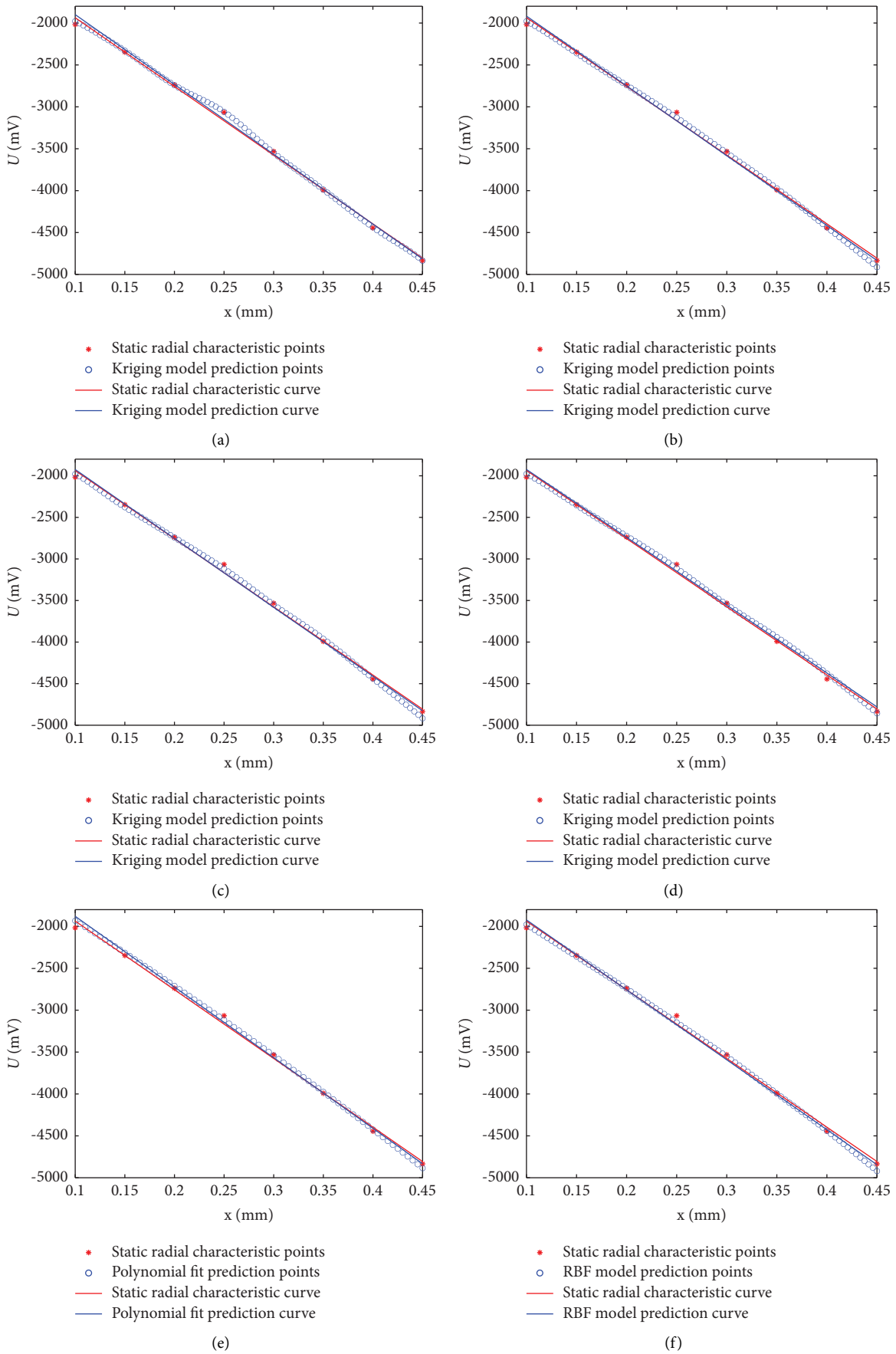

Figure 7: Comparison of the predicted curve and the experimental curve when the angle α of the blade cutting the magnetic field line is 17.825′: (a) Kriging model with 10 sets of sample points, (b) Kriging model with 6 sets of sample points, (c) Kriging model with 5 sets of sample points, (d) Kriging model with 3 sets of sample points, (e) polynomial fit of 10 sets of sampling points, and (f) RBF model with 6 sets of sampling points.

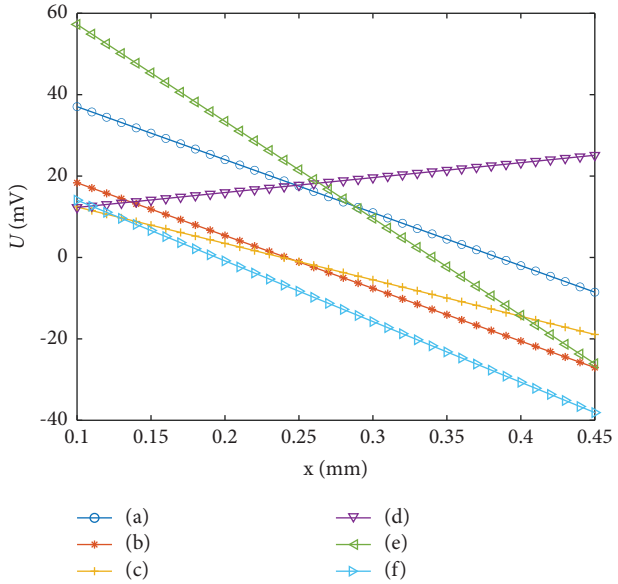

Figure 8: Comparison of the prediction error when the angle α of the blade cutting the magnetic induction line is 17.825′.

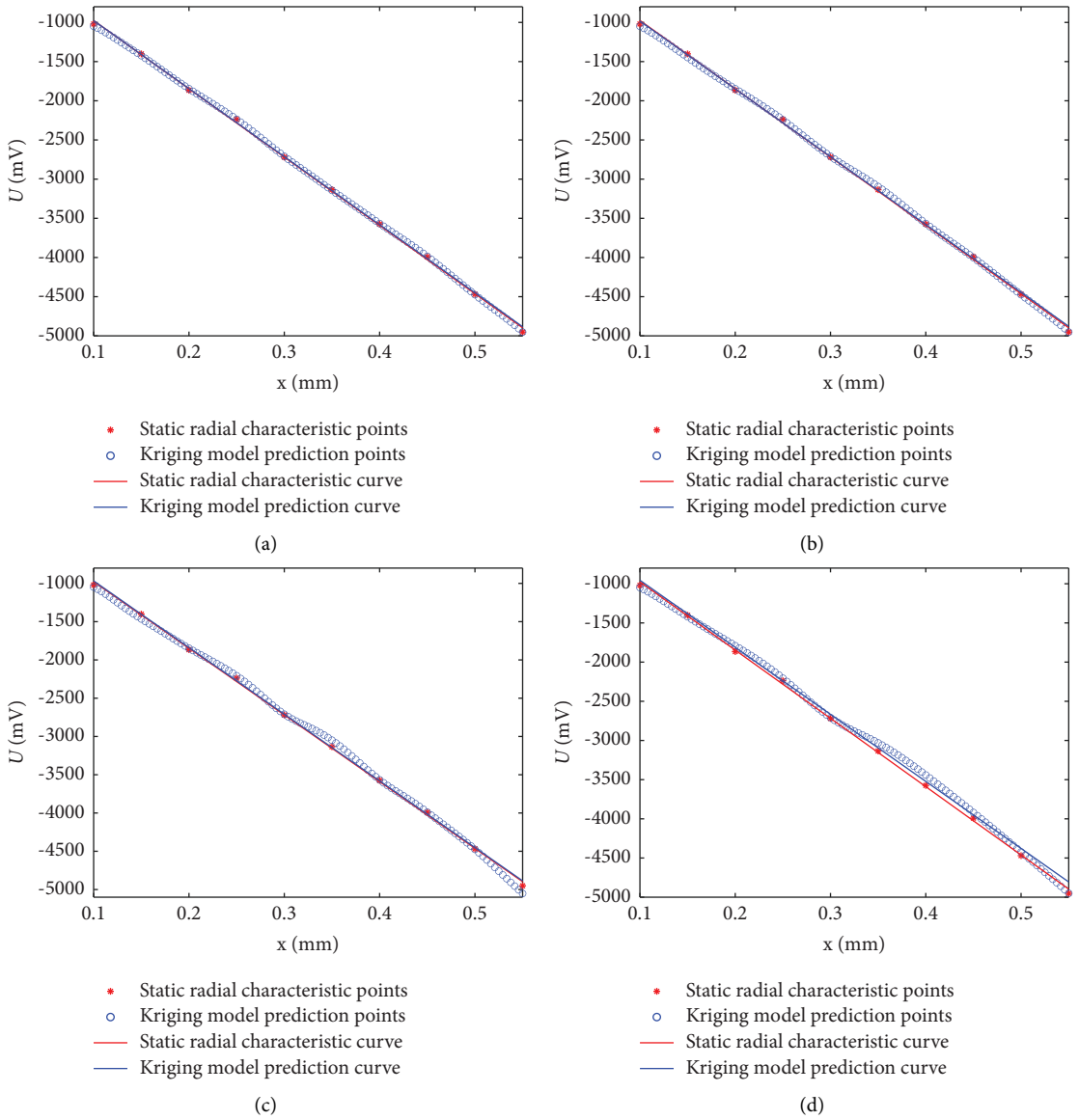

Figure 9: Continued.

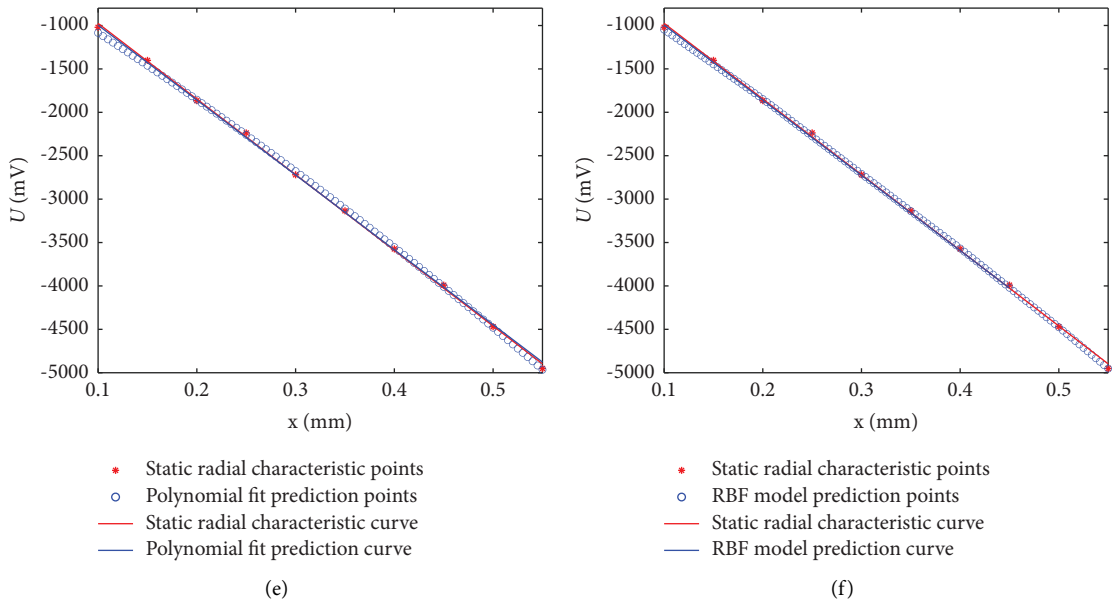

Figure 9: Comparison of the predicted curve and the experimental curve when the angle α of the blade cutting the magnetic field line is 35.65′: (a) Kriging model with 10 sets of sample points, (b) Kriging model with 6 sets of sample points, (c) Kriging model with 5 sets of sample points, (d) Kriging model with 3 sets of sample points, (e) polynomial fit of 10 sets of sampling points, and (f) RBF model with 6 sets of sampling points.

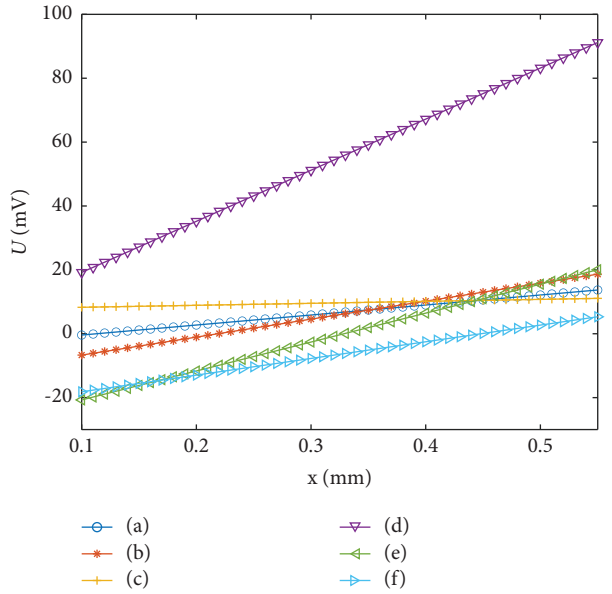

Figure 10: Comparison of the prediction error when the angle α of the blade cutting the magnetic induction line is 35.65′.

within the measurement error range of the eddy current sensor, indicating that both Kriging and RBF models have good prediction accuracy at this tip clearance. However, the prediction error of the Kriging model in Figure 11(d) is relatively large. When the Kriging model has only three sets of sample points, the prediction accuracy of the polynomial fit is better than that of the Kriging model. However, the prediction accuracy of the polynomial fit is slightly lower than that of the Kriging models with other sample points.

Next, at the tip clearance x of 0.15 mm, it is verified whether the insufficient prediction accuracy of the Kriging model in Figure 11(d) is caused by too few sample point groups in the model. When the tip clearance x is 0.15 mm, the comparison of the Kriging models prediction curves, the RBF model prediction curve, and the polynomial fit prediction curve with the static circumferential calibration curve obtained from the experimental data are shown in Figures 13(a)–13(f). In Figure 13(a), the static calibration

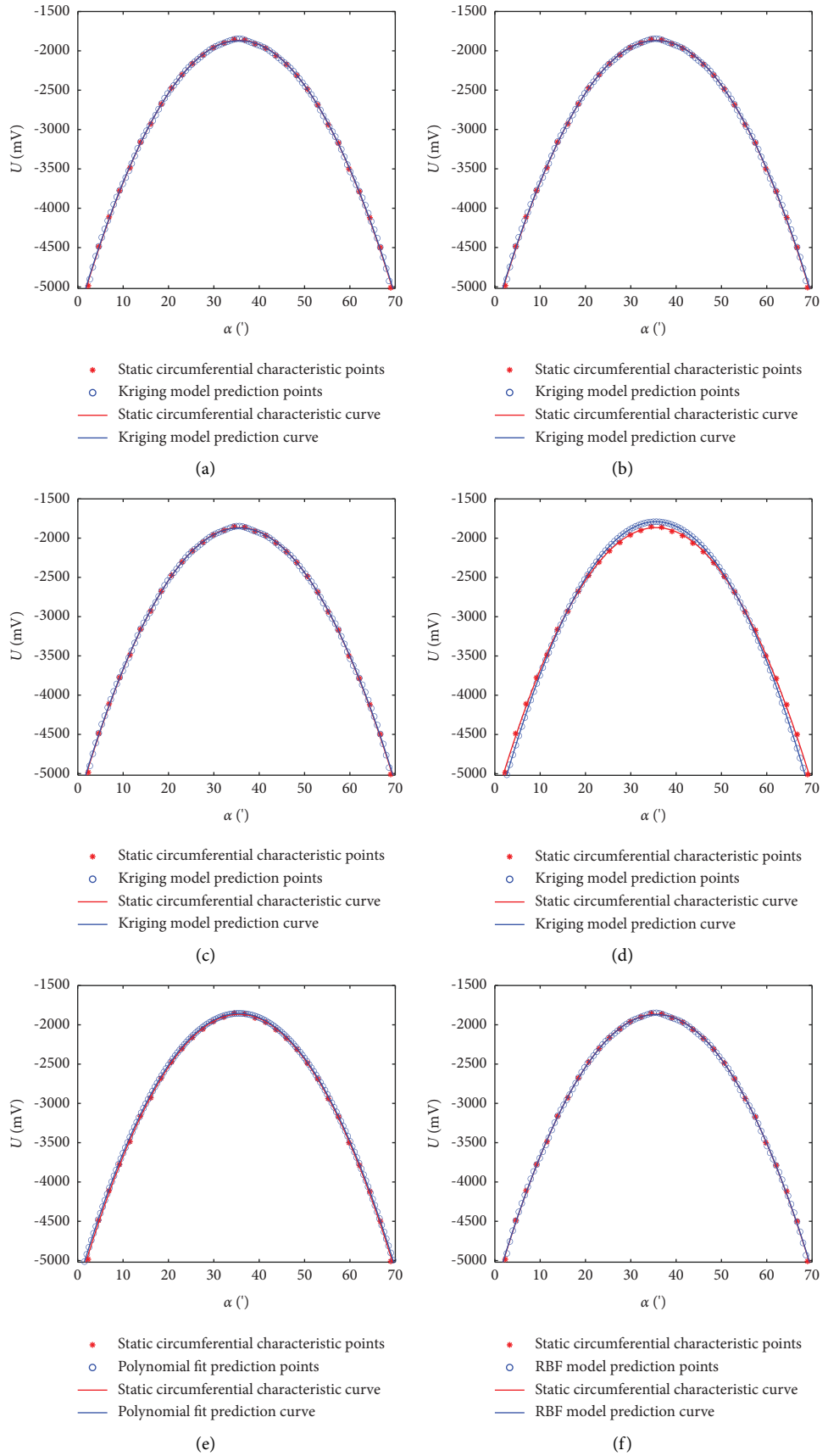

FIGURE 11: Comparison of the predicted curve with the experimental curve when the tip clearance x is 0.2 mm: (a) Kriging model with 10 sets of sample points, (b) Kriging model with 6 sets of sample points, (c) Kriging model with 5 sets of sample points, (d) Kriging model with 3 sets of sample points, (e) polynomial fit of 10 sets of sampling points, and (f) RBF model with 6 sets of sampling points.

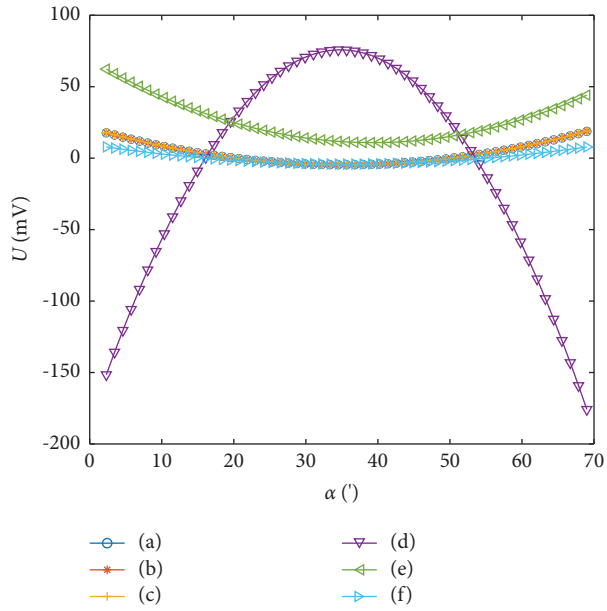

Figure 12: Comparison of prediction errors for a blade tip clearance x of 0.2 mm.

data for a 0.15 mm tip clearance has been input into the Kriging model, so the static circumferential characteristic curve predicted by the Kriging model in Figure 13(a) overlaps with the static circumferential calibration curve. In Figures 13(b)–13(d), the static circumferential characteristic curves predicted by the Kriging model also do not deviate significantly from the static circumferential calibration curves and still have a high degree of overlap. As can be seen in Figure 13(e), the polynomial fit prediction curve deviates significantly from the static circumferential calibration curve obtained from the experimental data, indicating that the polynomial fit cannot guarantee that a high prediction accuracy is maintained for all the data. In Figure 13(f), the static circumferential characteristic curve predicted by the RBF model is also in high agreement with the static circumferential calibration curve.

The comparison of prediction errors is shown in Figure 14. As shown in Figure 14, the Kriging model has high accuracy when predicting the location of the sample points. In other words, the closer the predicted data are to the location of the sample points, the higher the prediction accuracy of the Kriging model. When the predicted data are far away from the sample points, the prediction accuracy of the Kriging model decreases, and the maximum error gradually increases as the number of sample points decreases. With the same number of sample point sets, the prediction accuracy of the RBF model is slightly lower than that of the Kriging model, indicating that the Kriging model is more advantageous in predicting the

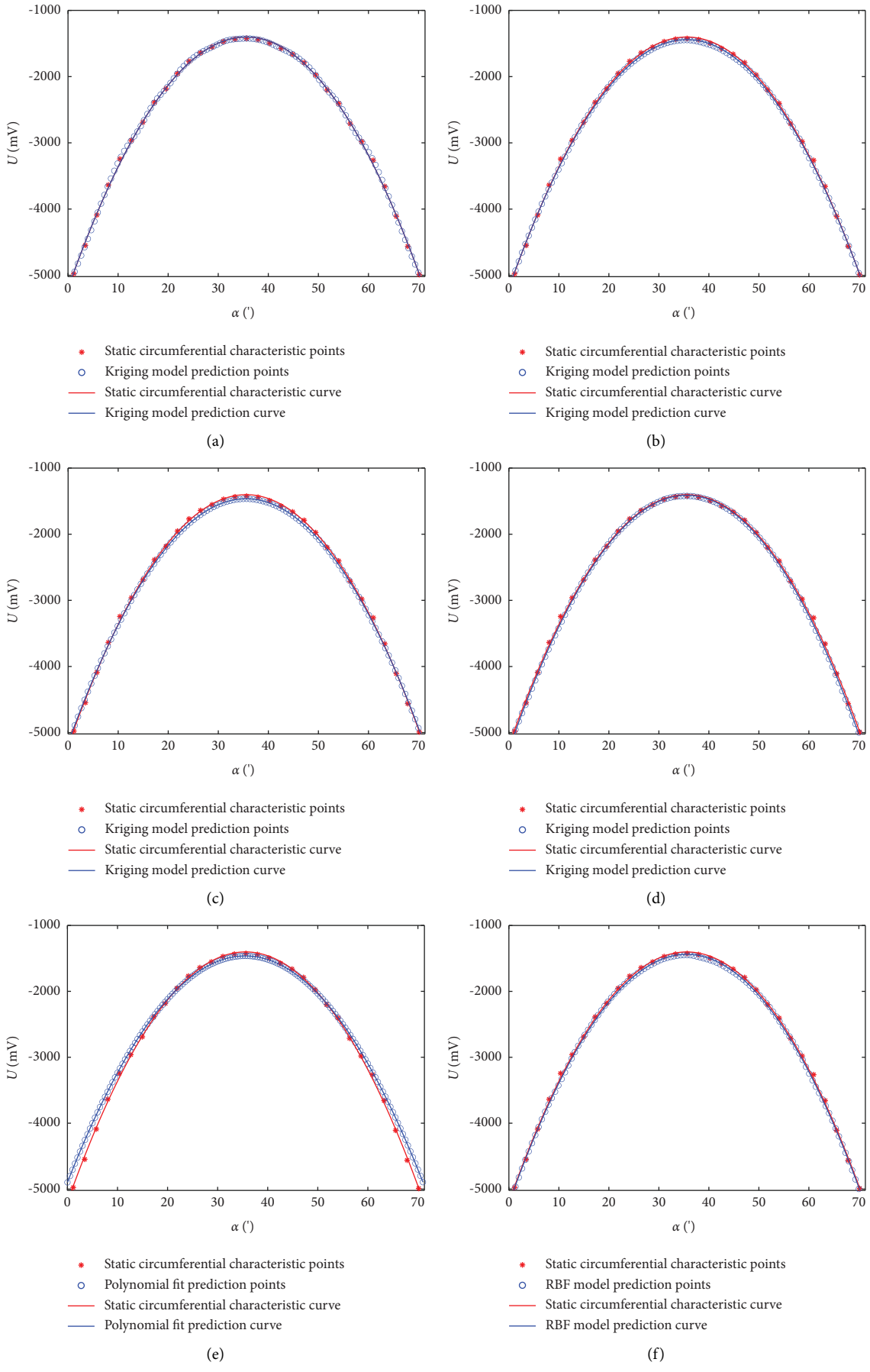

Figure 13: Comparison of the predicted curve with the experimental curve when the tip clearance x is 0.15 mm: (a) Kriging model with 10 sets of sample points, (b) Kriging model with 6 sets of sample points, (c) Kriging model with 5 sets of sample points, (d) Kriging model with 3 sets of sample points, (e) polynomial fit of 10 sets of sampling points, and (f) RBF model with 6 sets of sampling points.

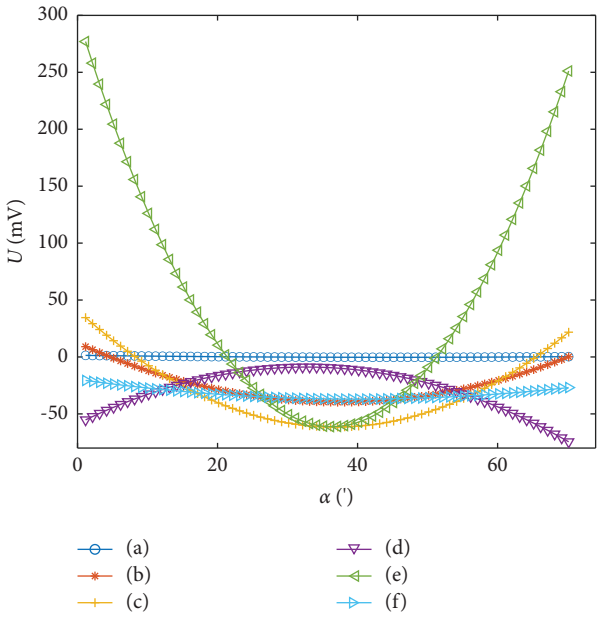

Figure 14: Comparison of prediction errors for a blade tip clearance x of 0.15 mm.

waveform under the unknown blade tip clearance. It indicates that the prediction accuracy of the Kriging model is affected when the number of sample point groups decreases, but it still has some accuracy. The Kriging model slightly outperforms the RBF model with the same number of sample points. In contrast, polynomial fitting does not guarantee highly accurate predictions for all data and is prone to significant prediction errors.

5. Conclusions

The numerical simulation is the main method for estimating blade tip clearance waveform under different operating conditions. However, it is difficult to accurately estimate the actual tip clearance waveform by obtaining theoretical simulation results of tip clearance under different working conditions. It is not easy to measure the experimental data of each tip clearance in the dynamic experiment. This article proposes a waveform prediction method for blade tip-timing sensor based on the Kriging model and static calibration data. Firstly, a static calibration test bench is established, and the static circumference calibration data obtained from the experiment under different tip clearances are used as the real values. Secondly, the polynomial fit prediction equation, the RBF prediction model, and the Kriging prediction model are established by changing the number of sample points, and their prediction accuracy is compared with the actual values obtained from experiments. The specific conclusions are as follows: the closer the predicted data are to the location of the sample point, the higher the prediction accuracy of the Kriging model. When the predicted data are far away from the sample point, the prediction accuracy of Kriging model decreases, but it still has high accuracy. If the number of sample points is too few, it would lead to the insufficient prediction accuracy of the Kriging model. Moreover, the Kriging model is less accurate when predicting points outside the sampling point range. Moreover, the prediction accuracy of the Kriging model is basically the same as that of the RBF model, but the Kriging model has more advantages in predicting waveforms under unknown blade tip clearance. In contrast, the prediction accuracy of the polynomial fit is lower than that of the Kriging and RBF models, and the polynomial fit is prone to significant prediction errors.

Data Availability

The data used to support the findings of this paper are available from the corresponding author upon request.

Conflicts of Interest

The authors declare that they have no conflicts of interest regarding the publication of this paper.

Acknowledgments

This article was supported by the National Natural Science Foundation of China (no. 51505206), Key Laboratory of Vibration and Control of Aero-Propulsion System, Ministry of Education, Northeastern University (no. VCAME202211), Liaoning Provincial Natural Science Foundation Guidance Program Project (no. 2019-ZD-0694), Liaoning Provincial Department of Education Scientific Research General Project (no. L2014246), and Liaoning University of Technology Teacher Research Start Fund Project (no. X201202). The authors are grateful to them.

References

[1] L. Witek, "Experimental crack propagation and failure analysis of the first stage compressor blade subjected to vibration," *Engineering Failure Analysis*, vol. 16, no. 7, pp. 2163–2170, 2009.

[2] S. Lavagnoli, C. De Maesschalck, and V. Andreoli, "Design considerations for tip clearance control and measurement on a turbine rainbow rotor with multiple blade tip geometries," *Journal of Engineering for Gas Turbines & Power*, vol. 139, no. 4, 2017.

[3] H. Jiang, H. F. Zuo, J. C. Guo, and Z. R. Zhong, "Electrostatic monitoring method for blade tip radial clearance of aero-engine," *Journal of Aerospace Power*, vol. 36, no. 3, pp. 466–476, 2021.

[4] B. Yu, H. W. Ke, E. Y. Shen, and T. H. Zhang, "A review of blade tip clearance-measuring technologies for gas turbine engines," *Measurement and Control*, vol. 53, no. 3-4, pp. 339–357, 2020.

[5] D. Mu¨ller, A. G. Sheard, S. Mozumdar, and E. Johann, "Capacitive measurement of compressor and turbine blade tip to casing running clearance," *Journal of Engineering for Gas Turbines & Power*, vol. 119, no. 4, pp. 877–884, 1997.

[6] Y. F. Xiong, "Rotor tip-clearance measurement in aero-engine," *Measurement & Control Technology*, vol. 1, pp. 5–7, 2004.

[7] I. García, J. Beloki, J. Zubia, G. Aldabaldetreku, M. A. Illarramendi, and F. Jiménez, "An optical fiber bundle

sensor for tip clearance and tip timing measurements in a turbine rig," *Sensors*, vol. 13, no. 6, pp. 7385–7398, 2013.

[8] C. P. Lawson and P. C. Ivey, "Tubomachinery blade vibration amplitude measurement through tip timing with capacitance tip clearance probes," *Sensors and Actuators A: Physical*, vol. 118, no. 1, pp. 14–24, 2005.

[9] J. W. Zhang, K. Q. Ding, and G. Chen, "High-precision extraction method for blade tip-timing signal with eddy current sensor," *International Journal of Rotating Machinery*, vol. 2020, Article ID 8882858, 13 pages, 2020.

[10] A. Maslovskiy, "Microwave turbine tip clearance measuring system for gas turbine engines," *Turbo Expo: Power for Land, Sea, and Air*, vol. 43123, pp. 105–114, 2008.

[11] W. K. Qi and W. Chen, "Tip clearance numerical analysis of an aero-engine HPT," *Journal of Nanjing University of Aeronautics & Astronautics*, vol. 35, no. 1, pp. 63–67, 2003.

[12] W. Shang, "Study on the condition monitoring and fault diagnosis of the gas turbine blade," Master's Thesis, Beijing University of Chemical Technology, Beijing, China, 2014.

[13] H. J. Shao, "Investigation on the turbine blade tip clearance measurement active clearance control and damping identification," Master's Thesis, Beijing University of Chemical Technology, Beijing, China, 2017.

[14] N. Jamia, M. I. Friswell, S. el-Borgi, and P. Rajendran, "Modelling and experimental validation of active and passive eddy current sensors for blade tip timing," *Sensors and Actuators A: Physical*, vol. 285, pp. 98–110, 2019.

[15] J. H. Cao, Z. B. Yang, H. Q. Li et al., "Rotating blade frequency identification by single-probe blade tip timing," *Mechanical Systems and Signal Processing*, vol. 172, Article ID 108961, 2022.

[16] C. Mandache, T. Mcelhinney, and N. Mrad, "Aircraft engine blade tip monitoring using pulsed eddy current technology," in *Proceedings of the 4th International Symposium on NDT in Aerospace*, pp. 1–12, Augsburg, Germany, November 2012.

[17] C. Liu and D. Jiang, "Improved blade tip timing in blade vibration monitoring with torsional vibration of the rotor," *Journal of Physics: Conference Series*, vol. 364, Article ID 012136, 2012.

[18] J. Wu, B. Wen, Y. Zhou et al., "Eddy current sensor system for blade tip clearance measurement based on a speed adjustment model," *Sensors*, vol. 19, no. 4, p. 761, 2019.

[19] A. Ariyarit, M. Sugiura, Y. Tanabe, and M. Kanazaki, "Hybrid surrogate-model-based multi-fidelity efficient global optimization applied to helicopter blade design," *Engineering Optimization*, vol. 50, no. 6, pp. 1016–1040, 2017.

[20] Z. H. Han and S. Görtz, "Hierarchical Kriging model for variable-fidelity surrogate modeling," *AIAA Journal*, vol. 50, no. 9, pp. 1885–1896, 2012.

[21] Y. P. Bu, W. P. Song, Z. H. Han, Y. Zhang, and L. Zhang, "Aerodynamic/aeroacoustic variable-fidelity optimization of helicopter rotor based on hierarchical Kriging model," *Chinese Journal of Aeronautics*, vol. 33, no. 2, pp. 476–492, 2020.

[22] L. K. Huang, Z. H. Gao, and D. H. Zhang, "Research on multi-fidelity aerodynamic optimization methods," *Chinese Journal of Aeronautics*, vol. 26, no. 2, pp. 279–286, 2013.

[23] J. Bailly and D. Bailly, "Multifidelity aerodynamic optimization of a helicopter rotor blade," *AIAA Journal*, vol. 57, no. 8, pp. 3132–3144, 2019.

[24] Q. Zhou, F. J. Duan, D. C. Ye, Y. Z. Li, and C. Xing, "Research on tip clearance measurement of steam turbine's interlocked blade based on eddy current sensor," *Instrument Technique and Sensor*, vol. 9, pp. 36–40, 2020.

[25] W. M. Wang, H. J. Shao, L. F. Chen, and W. Qu, "Investigation on the blade tip clearance monitoring of turbomachinery based on the pulse-trigger method," *Journal of Vibration, Measurement & Diagnosis*, vol. 37, no. 3, pp. 583–587, 2017.

[26] L. Zhang, Q. D. Wang, and X. Li, "An improved blade vibration parameter identification method considering tip clearance variation," *Shock and Vibration*, vol. 2021, Article ID 3537006, 14 pages, 2021.

[27] L. Zhang and X. Li, "Thermal-fluid-structure interaction analysis of bladed disk system based on Kriging model and hypothetic elastomer method," *International Journal of Manufacturing Research*, vol. 12, no. 2, pp. 253–269, 2017.

[28] J. J. Ma, H. Yin, Z. R. Peng, and K. L. Dong, "Damage identification method based Kriging model," *Journal of Mechanical Strength*, vol. 42, no. 4, pp. 786–792, 2020.